THE JOURNAL OF PHYSICAL CHEMISTRY C

Article

pubs.acs.org/JPCC

Electrochemical CO_2 and CO Reduction on Metal-Functionalized Porphyrin-like Graphene

Vladimir Tripkovic, Marco Vanin, Mohammedreza Karamad, Mårten E. Björketun, Karsten W. Jacobsen, Kristian S. Thygesen, and Jan Rossmeisl*

Center for Atomic-scale Materials Design, Department of Physics, Technical University of Denmark, DK-2800 Kongens Lyngby, Denmark

Supporting Information

ABSTRACT: Porphyrin-like metal-functionalized graphene structures have been investigated as possible catalysts for CO_2 and CO reduction to methane or methanol. The late transition metals (Cu, Ag, Au, Ni, Pd, Pt, Co, Rh, Ir, Fe, Ru, Os) and some p (B, Al, Ga) and s (Mg) metals comprised the center of the porphyrin ring. A clear difference in catalytic properties compared to extended metal surfaces was observed owing to a different electronic nature of the active site. The preference to bind hydrogen, however, becomes a major obstacle in the reaction path. A possible solution to this problem is to reduce CO instead of CO_2. Volcano plots were constructed on the basis of scaling relations of reaction intermediates, and from these plots the reaction steps with the highest overpotentials were deduced. The Rh−porphyrin-like functionalized graphene was identified as the most active catalyst for producing methanol from CO, featuring an overpotential of 0.22 V. Additionally, we have also examined the hydrogen evolution and oxidation reaction, and in their case, too, Rh−porphyrin turned out to be the best catalyst with an overpotential of 0.15 V.

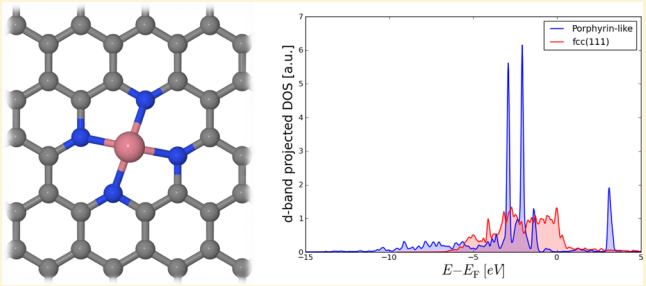

I. INTRODUCTION

The intermittency of renewable energy sources calls for a practical energy storage solution.[1,2] This can be accomplished by finding an efficient way to store energy in the form of chemical fuels, which would be particularly appealing if combined with CO_2 capture. For that reason, the electrochemical reduction of CO_2 to chemical fuels has spurred huge interest in recent years.[1−20] Copper is the only metal that has been experimentally shown to produce significant quantities of hydrocarbons, mostly CH_4 and C_2H_4, albeit at a huge voltage cost and with a low faradaic efficiency due to the competing hydrogen evolution reaction.[3−5,7,21,22] Furthermore, none of the metals was able to produce methanol. The origin of the overpotential remained elusive until recently, when a complete reaction mechanism was mapped out by employing density functional theory (DFT) calculations in conjunction with the computational hydrogen electrode method.[18,19,23]

The lack of efficient metallic catalysts for the electrochemical reduction of CO_2 necessitates scrutiny of other types of materials. We have studied a new class of materials consisting of a metal atom coordinated to a porphyrin ring embedded in graphene (cf. Figure 1a). The term "porphyrin-like" has been used in order to emphasize that our structure differs from the usual porphyrin structure: the central metal atom is coordinated to four nitrogen atoms and with neighboring carbon atoms forms five- and six-atom-long rings. This particular 4-fold coordination was chosen because it was found to be the most stable binding configuration for metal and nitrogen atoms in graphene.[24−26]

Recent advances in experiments have made it possible to synthesize nanostructured graphene. Graphene sheets can be readily doped and modified for catalytic and energy conversion purposes.[27−29] The porphyrin type of functionalization has already been realized experimentally on carbon nanotubes and other graphitic materials. Some of these systems have been shown to possess high catalytic activities for oxygen reduction and methanol oxidation reaction.[24,25,30−33]

The choice of catalysts was inspired by two facts: first, some porphyrin-based catalysts are known to be active for electrochemical reduction of CO_2;[34−37] second, the versatility and relatively low cost of graphene render the studied system a very good catalyst candidate.

The sine qua non condition to make CO_2/CO reduction cost efficient is to find a suitable catalyst. A good catalyst should fulfill three criteria: (1) it should be active in reducing CO_2/CO, i.e. have a low reduction overpotential, (2) it should have a high faradaic efficiency toward CH_4/CH_3OH, and (3) it should be stable, i.e., not poisoned by adsorbed H or OH. The aim of this work is to investigate if any of the studied systems fulfills these three basic conditions.

Received: June 22, 2012
Revised: April 10, 2013
Published: April 10, 2013

   dx.doi.org/10.1021/jp306172k | J. Phys. Chem. C 2013, 117, 9187−9195

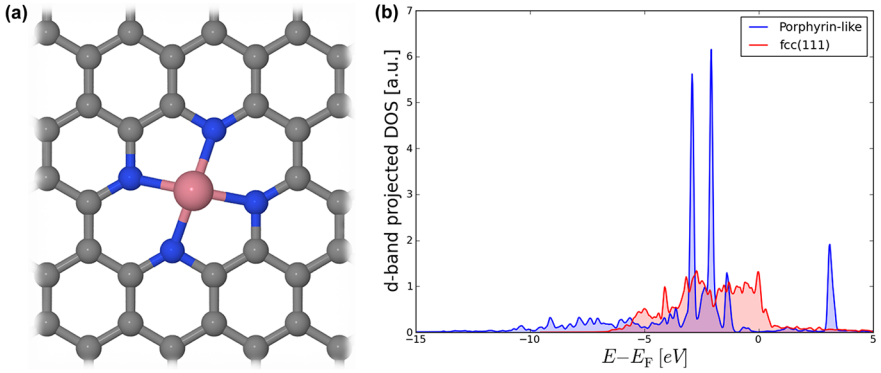

Figure 1. (a) Atomic structure of porphyrin-like functionalized graphene. The central metal atom is coordinated to four nitrogen atoms, forming the porphyrin ring that is embedded in a graphene matrix. (b) Comparison of density of states projected onto the d orbitals of the Pt atom located at the center of the porphyrin ring and the Pt surface atom in Pt(111) surface.

Electronically, a single, isolated, active site is in stark contrast to traditional metal-based catalysts where often many active sites are available for intermediates to bind. This difference is visualized in Figure 1b, in which the total density of states (DOS) is projected onto the d orbitals of Pt in the porphyrin-like graphene and the d orbitals of Pt in the Pt(111) surface, respectively. As can be seen, the graphene system exhibits more atomic-like, sharp peaks compared to the broad d-band features of the extended metal surface. The huge disparity in the DOS could have a significant impact on the catalytic activity. Distinct features offered by an individual active site can be seen as a bridge between a metal-based catalyst and a molecular catalyst, and it can open up an ample spectrum of possibilities in terms of engineering and controlling the active site.

II. COMPUTATIONAL METHODS

The electronic structure calculations were carried out with use of DFT based on the projector augmented wave method and the revised Perdew–Burke–Ernzerhof (RPBE)[38] functional. The calculations were performed spin polarized with the use of the real space GPAW software package[39,40] integrated with the Atomic Simulation Environment (ASE).[41] The functionalized porphyrin-like structures were modeled in a 4 × 4 graphene unit cell using periodic boundary conditions and sufficient vacuum in the direction perpendicular to the graphene plane (at least 12 Å). A grid spacing of 0.18 Å and a (8 × 8 × 1) *k*-point sampling grid were employed. All the structures were relaxed until the force on each atom was lower than 0.01 eV/Å. We have used the computational hydrogen electrode (CHE) method to calculate the free energy levels of all the intermediate states and to construct the potential energy diagrams.

The rationale behind the CHE method is to calculate electrochemical reactions as if they were chemical using the definition of the standard hydrogen electrode (SHE, $H^+ + e^- = H_2$), and then afterward to correct for conditions other than standard. In this manner, the cumbersome problem of calculating charges and ions in solution is neatly replaced by a much simpler problem of computing hydrogen in the gas phase. Conceptually, the CHE method can only deal with concerted electron–proton transfer. The systems are computed at $U = 0$, and afterward, all the states are tuned to a desired voltage by changing the free energy by eU, where U is the electrode potential. Similarly, the pH effects are not directly taken into account (values are given on the reversible hydrogen electrode (RHE) scale), but they can be accounted for a posteriori by changing the chemical potential of protons. Applying the CHE method assumes an aqueous environment as, by definition of the SHE, protons are solvated in water and not in some other medium. To include solvation effects, we use a simple thermodynamic correction of 0.3 eV[55] for all species that contain an OH group (OH, COOH, COH, CHOH, CH_2OH). We have not probed the influence of the electric field on the binding energies because previous studies have shown that it has a very limited effect on the overall results.[56−58] For more details about this approach we refer to ref 23, in which the method was initially outlined. Also, we would like to emphasize that this is a purely thermodynamic study: charge transfer kinetics have not been taken into account. However, according to previous studies on metals,[59] the kinetics should not play a significant role. Additionally, knowing how water adheres on the surface is a prerequisite for studying kinetics, but this has yet to be ascertained.

Discussion about the Method. In this section we present arguments why we deem our method suitable for studying these systems.

Porphyrin molecules are well-known to the organometallic community, and they have been the main targets for photocatalytic application for decades. However, the methods they used are inherently different from the one employed here because they all reside in the fact that electron–proton transfer is treated independently. For molecular catalysts solvated in water or some other medium, the only way to activate the metal center toward CO_2/CO reduction is to lower the potential in order to allow the electrons from the neighboring ligand groups to occupy the lowest unoccupied molecular orbital (LUMO) state of the molecule. Since, usually their LUMO state lies far from the Fermi level, the overvoltage requirement is significant, and the electron transfer becomes a major obstacle.[42−44] Therefore, the electron transfer is considered independently from the proton transfer, which is seen to be a more facile step. The metal atom in the porphyrin ring can undergo only discrete changes from one valence state to another, which is usually handled by calculating the redox potentials. In contrast, our systems should be considered as a whole, in which porphyrin motifs are part of a larger graphene electrode. There is no need to look at decoupled proton–electron transfer as there are always available graphene or/and metal states just above the Fermi level (see Supporting Information, Figure 4) that can be readily occupied at negative potentials. In other words, while the charge in molecular catalysts is centered on the porphyrin ring, in our systems it is spread out all over the

dx.doi.org/10.1021/jp306172k | J. Phys. Chem. C 2013, 117, 9187−9195

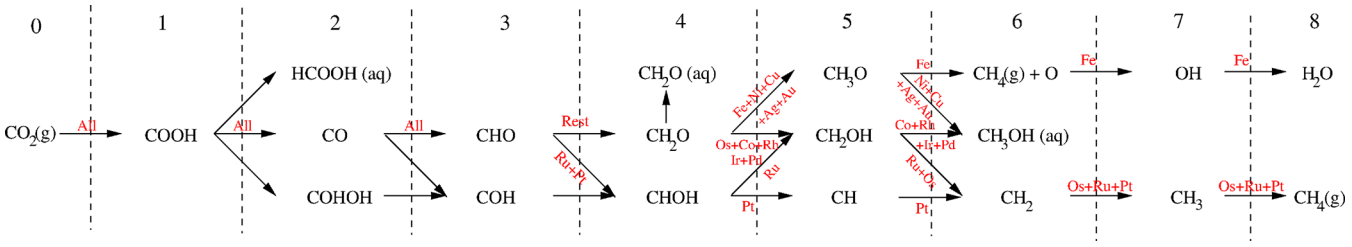

Figure 2. Reaction paths for electrochemical CO_2 reduction on a range of d metals. "All" and "Rest" labels stand for all and remaining metals.

graphene−porphyrin electrode. By changing the potential, one would change not the oxidation state of the atom, but rather the surface dipole of the electrode. The surface dipole would change continuously in the same way as the chemical potential—the variable it depends on. Consequently, the binding energies would also change linearly with potential. Since there are no experimental results for CO_2/CO reduction to support this claim, we will refer to another reaction, that is, the oxygen reduction reaction extensively studied on the same/similar type of catalysts.[45,46] The continuous current−potential curves without any abrupt features in cyclic voltammograms give evidence that the graphene−porphyrin system behaves as one electrode.

We have chosen the RPBE functional because it gives good oxidation states for metal atoms in the porphyrin ring, assuming square-planar geometry and corresponding splitting of the d states.[47,55] However, this functional is also known to favor low spin states for transition metals with partially filled 3d orbitals.[48−51] To get the right spin state, one would need to employ a hybrid GGA functional; however, this is out of the scope of this paper. We believe that the chosen functional is sufficiently accurate for the purpose of this study, which is to report activity trends, although we do not exclude the possibility that some of the 3d metals might shift on the volcano plots. Furthermore, all the calculations are performed spin polarized, assuming the porphyrin motifs to be ferromagnetic. This might not always be true: a recent study has shown that two adjacent porphyrin motifs can have opposite spins;[26] i.e., the overall system can become antiferromagnetic. Nevertheless, the energy differences were too minute (on the order of millielectronvolts) to add any significant error bar to our calculations. The binding energies will also be affected by the choice of the exchange-correlation functional;[52] however, as almost all the species have very similar electronic structures with the highest occupied molecular orbital (HOMO) state at nearly the same position (see the Supporting Information Figures 6 and 7 for more details), the binding energies will change proportionally, having little or no effect on the volcano plots.

Additionally, we would like to emphasize that we used a correction for the DFT-RPBE value of CO_2(g) in GPAW. It has previously been established that the RPBE functional does not yield good reaction energies for reactions that contain CO_2(g) or gas phase molecules with a CO_2 group.[18] Analyzing the same set of gas phase reactions as in ref 18, we arrived at a CO_2/CO correction of 0.43/0.04 eV (see the Supporting Information for detailed information). Subsequently, all the CO_2(g) energies were corrected by this amount, while the CO(g) correction was neglected.

Finally, we have just looked at thermodynamic barriers; for calculating charge transfer barriers one needs to explicitly include water in the system.[53,54]

III. RESULTS AND DISCUSSION

The electrochemical CO_2 reduction reaction (CRR) is a many proton−electron transfer step process that entails a lot of different reaction intermediates with several possible reaction outcomes. The final product depends on the number of reduction steps, which is in general determined by the strength of the CO binding.[2] The most common reactions and their equilibrium potentials vs RHE are listed below.

$$CO_2 + 2H^+ + 2e^- \rightarrow HCOOH(aq) \qquad (U = -0.20\ V)$$

$$CO_2 + 2H^+ + 2e^- \rightarrow CO + H_2O \qquad (U = -0.12\ V)$$

$$CO_2 + 4H^+ + 4e^- \rightarrow CH_2O(aq) \qquad (U = -0.07\ V)$$

$$CO_2 + 6H^+ + 6e^- \rightarrow CH_3OH(aq) \qquad (U = 0.03\ V)$$

$$CO_2 + 8H^+ + 8e^- \rightarrow CH_4 \qquad (U = 0.17\ V)$$

The two most valuable products are methanol and methane; however, as mentioned in the Introduction, only Cu is able to reduce CO/CO_2 to hydrocarbons, whereas none of the metals was seen to produce methanol in significant amounts. We have systematically analyzed, based on DFT simulations, all possible reaction pathways (cf. Figure 2) for CRR on a range of different metals in the porphyrin ring (Cu, Ag, Au, Ni, Pd, Pt, Co, Rh, Ir, Fe, Ru, Os, B, Al, Ga, and Mg).

The number of possible intermediates and reactions is reduced compared to metal surfaces as the single active site can only bind one intermediate at a time. Accordingly, methane and methanol are the only hydrocarbon and alcohol that can be produced. Making larger hydrocarbon chains would require a Langmuir−Hinshelwood reaction in which two adsorbed species join together to form a C−C bond.

Selectivity Criteria. As already discussed, in this class of materials catalytic sites are isolated from each other. Their distribution is uniform owing to the imposed periodic boundary conditions. The existence of only one active site simplifies the theoretical analysis because no coverage effects need to be taken into account. On the other hand, the competition for the active site, i.e., selectivity, enters as a key parameter that determines the overall performance of the catalyst. Similarly, if some of the intermediates that are not directly involved in CRR path would bind stronger to the surface, they would poison the active site and thus terminate the reaction. All potential reaction pathways, except for the hydrogen evolution reaction (HER), proceed through the COOH* intermediate, and therefore the competition between H* and COOH* binding will determine the outcome of the reaction. Moreover, as both the H* and the COOH* formation steps involve transfer of one proton−electron pair, the difference between the H* and COOH* binding energies is not affected by the change in voltage.

dx.doi.org/10.1021/jp306172k | J. Phys. Chem. C 2013, 117, 9187−9195

To further investigate the impact of HER, the binding energies of the first intermediates in HER and CRR, H* and COOH*, were plotted against each other in Figure 3a. Ideally, the points should fall in the lower part of the graph, in which the H* blockage would not impede CRR ($G_{COOH^*} < G_{H^*}$). However, from the figure it is clear that CRR would be completely suppressed by hydrogen adsorption in almost all the systems.

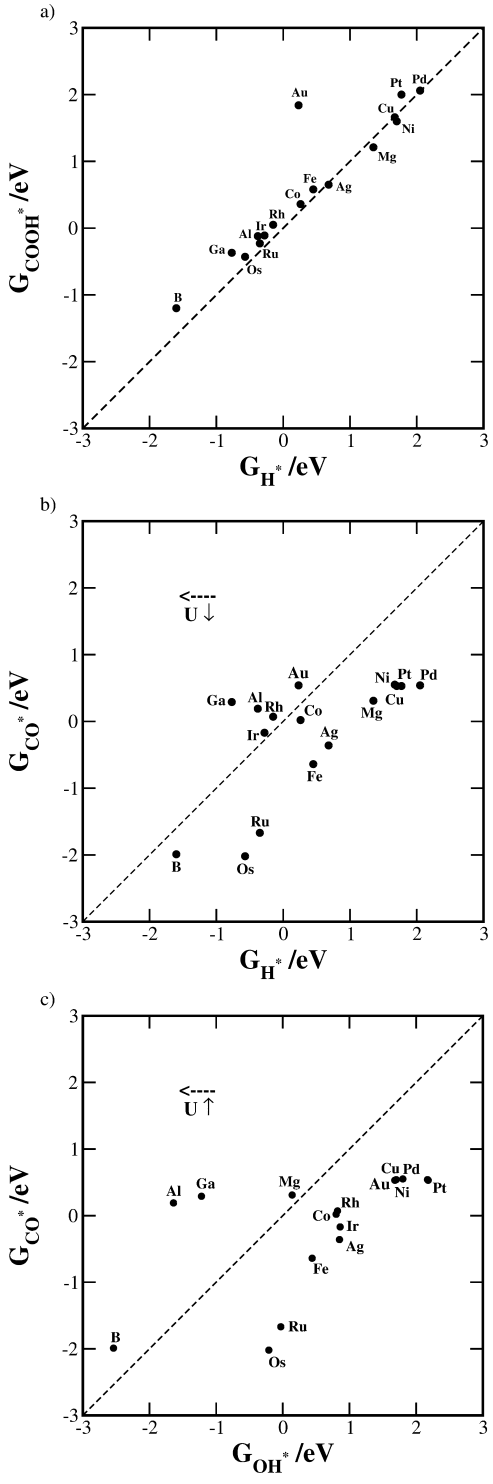

Figure 3. Selectivity criteria defining preference toward HER or CRR. The COOH* and CO* binding energies are calculated with respect to $H_2O(l)$, $H_2(g)$, and the energy of the C-containing molecule they originate from, that is, $CO_2(g)$ for COOH* and CO(g) for CO*, respectively. The horizontal arrows show how the binding energies of H* and OH* species change with respect to a change in potential (vertical arrows).

The reaction diagram in Figure 2 suggests a way to overcome the hydrogen poisoning problem. If one would reduce CO instead of CO_2, then the weak COOH* binding might no longer present a hindrance. Moreover, CO can be used as a viable alternative to CO_2 because it is a product of many industrial processes such as gasification of biomass, cracking of hydrocarbons, or metal oxide reduction. Alternatively, CO could be produced from CO_2 by a process opposite to the water gas shift reaction or, perhaps, even electrochemically using some other catalyst to reduce CO_2 to CO. The CO reduction follows the same path as the CO_2 reduction apart from the first two steps that are missing. CO* is expected to bind stronger than COOH* and, thus, to better compete with H*. It is clear from Figure 3b that the CO* binding is stronger on most of the metal atoms at $U = 0$ V vs RHE. The CO* binding is potential independent, while the free energy of the $H^+ + e^- \rightarrow H^*$ reaction changes as a function of the applied voltage. When the potential is reduced, the points will shift accordingly to the left in Figure 3b. For the points that lie close to the diagonal, at negative potentials the selectivity will change toward HER. A way to work around this problem could be to cycle the cell potential. To better explain this approach, let us take an example, for instance Rh−porphyrin. The Rh point is located slightly on the left side of the diagonal, meaning that at a very small positive potential the selectivity will turn toward the CO reduction products. However, as CO cannot be reduced at positive potentials, the voltage needs to be lowered to enable CO reduction. Hence, the CO reduction could be accomplished by periodically cycling the potentials in the cell between the potentials at which CO adsorbs and the potentials at which it reduces.

Brief excursions to positive potentials can bring another problem: water oxidation and subsequent OH* poisoning of the active site. To elucidate this possibility, we have plotted the CO* vs OH* binding energies for all the metals in Figure 3c. When the potential is increased above $U = 0$ V, the OH* binding shifts to the left; i.e., the OH* species become more stable on the surface. According to Figure 3c, the OH* poisoning presents a problem only for Ga, B, Mg, and Al as all the other metals lie at a safe distance from the diagonal.

In the following discussion we will restrict our analysis to the transition metals, although we show results for all the metals used in this study.

Scaling Relations and Volcano Plots. For a multielectron transfer reaction, it is usually difficult to find a good catalyst that can perform the overall reaction at a small voltage cost. This is best illustrated by comparing electrochemical reactions that involve different numbers of proton−electron transfer steps. Complete reductions of hydrogen, oxygen, and CO_2 proceed through two, four, and eight charge transfer steps; at the same time their smallest predicted overpotentials change from 0, to 0.4, to 0.9 V.[18,23,59,60] The large differences in overpotentials can be understood in terms of the intermediates' binding energies, which are commonly found to scale linearly against each other.[61] The scaling relations are not only limited to metallic surfaces, but as was recently shown also hold on graphene, at least for oxygen reduction intermediates.[47,55] The linearity in binding energies on transition metals is usually rationalized through the d-band model and the position of the

dx.doi.org/10.1021/jp306172k | J. Phys. Chem. C 2013, 117, 9187−9195

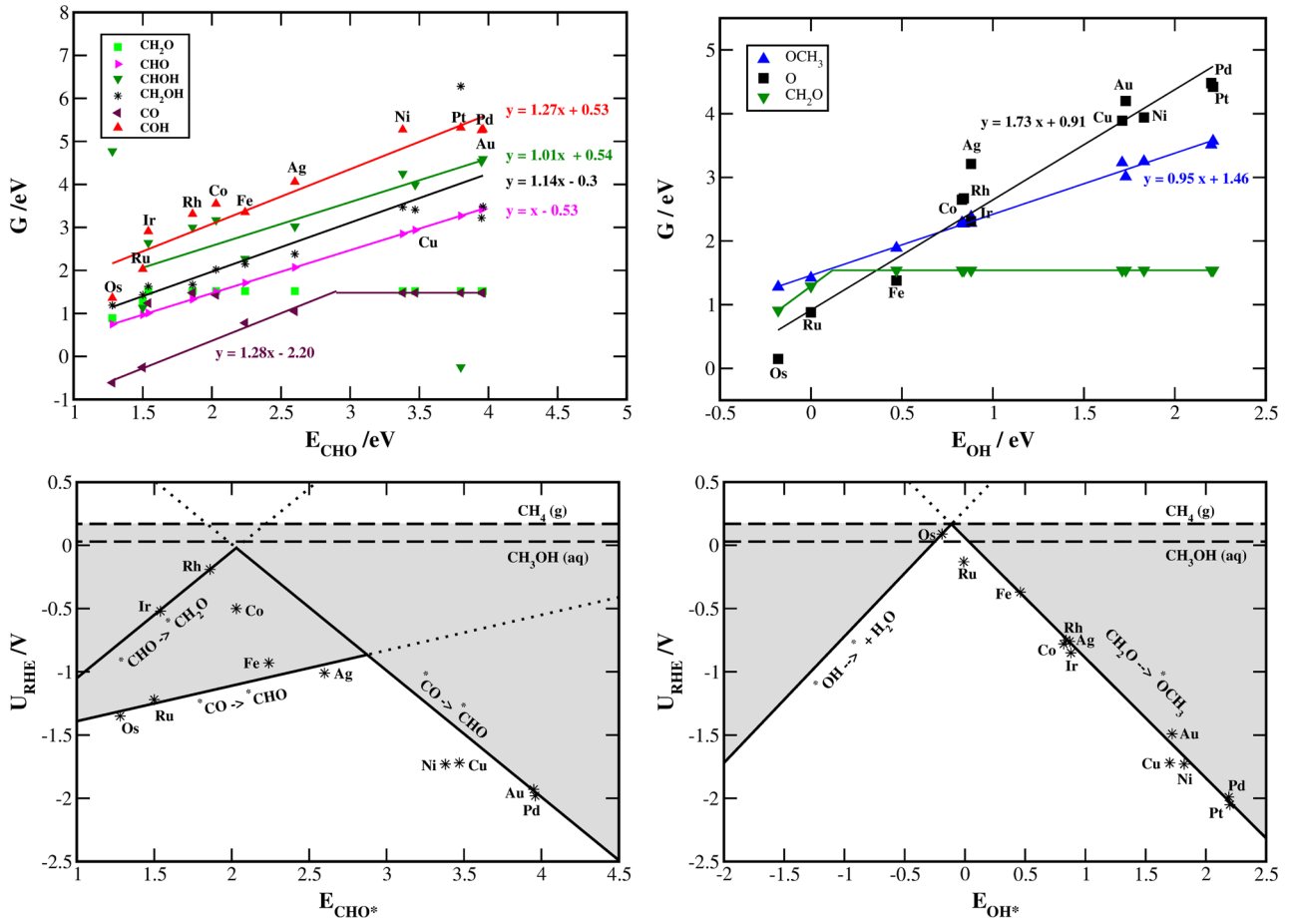

Figure 4. Scaling relations and volcano plots indicating potential determining steps for CO electroreduction. The gray areas designate the overpotentials for this class of catalysts. They stretch from the equilibrium potentials for methanol and methane production, 0.03 and 0.17 V, respectively, to the minimum potential required to drive the reaction at different CHO* and OH* values (solid black lines). The overpotential for CO reduction is the bigger value in the two volcano plots.

d-band center.[62] It is impossible to change the binding energy of one intermediate without simultaneously affecting the binding of others in a proportional manner. Tuning an eight electron transfer reaction such as CRR is therefore a cumbersome task.

Reduction of CO results in three possible products: formaldehyde, methanol, and methane. Most of the metal-functionalized porphyrin-like catalysts produce formaldehyde, CH_2O. As CH_2O is just an intermediate product in the full reduction path, it could be easily further reduced to methanol or methane.

In Figure 4 all the intermediates appearing in the main reaction path are plotted versus either CHO* or OH* binding energies, depending on whether the species bind through carbon or oxygen atoms. It is important to stress, here, why we have chosen to scale the intermediates' binding energies against CHO* and not against CO*, which is commonly used as a descriptor in reactions containing C_xO_y species. The problem with CO* is that it does not bind on all the metals, and consequently, those metals will not show up in the scaling relations. This is not the case on extended metal surfaces because most of the metals bind CO. CHO* is the most obvious choice, not just because it binds on all the metals, but also because all reaction paths lead through this intermediate.

The scaling relation for CH_2O* is a broken line, since on most metals CH_2O* desorbs from the surface (exceptions are Ru and Os). A few metals that substantially deviate from other points were not included in the fits (e.g., Pt in CHOH and CH_2OH scalings). Another important observation is that the slopes of the lines in the CHO* scaling plot fall close to 1.00 (1.01−1.27). This result is different from what could be expected if the bond counting rule established on metal surfaces is applied.[61] According to this simple rule, the expected slopes for the CH_2OH*, CHOH*, and COH* scalings against the CHO* should be 1, 2, and 3 because they should in principle form one, two, and three bonds to the metal atom, whereas CHO* should bind through a single bond. The reason why the slopes defy the bond counting rule is because the species can just bind to a single atom. The intermediates cannot satisfy their unpaired electrons as there are no metal aggregates available on the surface. This interpretation is corroborated by the DOS analysis reported in the Supporting Information. The only exception is the oxygen intermediate, most likely because oxygen has the highest electronegativity, so it can drain more charge from the metal atom.

By using linear relationships, we have constructed volcano plots, shown as well in Figure 4. All energies were corrected by free energy corrections calculated on the Cu(211) surface.[18] Although the geometries of the intermediates might vary between those on Cu(211) and metal-functionalized porphyrin-like graphene, the zero point energies and entropies will not be appreciably affected. For more details on the construction of

dx.doi.org/10.1021/jp306172k | J. Phys. Chem. C 2013, 117, 9187−9195

volcano plots, we refer to ref 63. In most systems the potential determining step (PDS) is found in the CHO volcano. Notice also that the CO* reduction to CHO* gives rise to both the left and right leg of the volcano. The difference between the CO (brown) and CHO (magenta) trend lines in the CHO scaling plot is in fact what yields the CHO volcano. The CHO volcano describes well the overpotentials for all the points except for Rh, Ir, and Co. These metals deviate substantially from the linear trend because either they do not bind CO (Co, Rh) or they bind it very weekly (Ir). Consequently, these metals exhibit different PDS: for Rh and Ir it is the CHO* reduction to CH_2O, whereas for Co it is the CH_2O reduction to CH_2OH*. Owing to relatively large deviations Rh, Ir, and Co seem to be very good catalysts for CO reduction. This result corroborates, once again, the claim that one of the ways to beat large overpotentials is to have points that do not obey general trends.

The early transition metals were not included in the study because shifting to stronger binding energies would only increase the overpotential in the CHO volcano.

Whether the final product of the reaction is methane or methanol depends on the central metal atom in the porphyrin ring. Table 1 shows what the most stable product on different metals is, the potential at which the reduction takes place, and PDS. As seen, two-thirds of the metals produce methanol and one-third produce methane. PDS are either the CO/CHO reduction to CHO/CH_2O in the CHO volcano or the CH_2O reduction to CH_3O in the OH volcano. The exceptions are the p-metals B, Al, and Ga, presumably because they follow different trends.

Table 1. Calculated Potentials for the CO_2 Reduction Reaction, Main Reaction Product, and PDS[a]

metal	path	potential (V)	PDS
Cu	CH_3OH	−1.72	$CH_2O(aq) \rightarrow CH_3O$
Ag	CH_3OH	−1.01	$CHO^* \rightarrow CH_2O(aq)$
Au	CH_3OH	−1.94	$CO^* \rightarrow CHO^*$
Ni	CH_3OH	−1.73	$CH_2O(aq) \rightarrow CH_3O$
Pd	CH_3OH	−1.99	$CH_2O(aq) \rightarrow CH_3O^*$
Pt	CH_4	−6.32	$CHOH^* \rightarrow CH^*$
Co	CH_3OH	−0.20	$CH_2O(aq) \rightarrow CH_2OH^*$
Rh	CH_3OH	−0.19	$CHO^* \rightarrow CH_2O(aq)$
Ir	CH_3OH	−0.52	$CHO^* \rightarrow CH_2O(aq)$
Fe	CH_4	−0.93	$CO^* \rightarrow CHO^*$
Ru	CH_4	−1.22	$CO^* \rightarrow CHO^*$
Os	CH_4	−1.35	$CO^* \rightarrow CHO^*$
Mg	CH_3OH	−1.29	$CO^* \rightarrow CHO^*$
Al	CH_4	−1.17	$CH_3O^* \rightarrow O^*$
Ga	CH_4	−0.94	$CH_3O^* \rightarrow O^*$

[a]The overpotential for methanol or methane formation is obtained by adding the reactions' equilibrium potentials to the absolute potentials in the table.

The best catalyst for the reaction is the system with the lowest max(U_{RHE}(CO), U_{RHE}(OH)). In our case this is Rh, which exhibits only 0.19 + 0.03 = 0.22 V overpotential (0.19 V is the potential at which CO reduces and 0.03 V is the equilibrium potential for the CO reduction to methanol). As a comparison, on the most active metal surface, Pt(111), the requirement for CO reduction to methanol is 0.46 V,[64] and on the most active step surface, Cu(211), it is 0.77 V.[18] Figure 5 shows the free energy diagram for the CO reduction on Rh together with snapshots of the most stable structures in each electrochemical step.

Hydrogen Oxidation/Evolution Reaction. So far we have considered HER only in terms of hydrogen poisoning and its implications on the CRR; however, HER is an important reaction in itself. This reaction, for instance, takes place at the cathode of a water electrolyzer—a device that is able to convert solar into chemical energy by splitting water into its constituents.[1] The opposite reaction to HER, the hydrogen oxidation reaction (HOR), is perhaps even more important because it is a major reaction in fuel cells. Pt is the state-of-the-art catalyst for HER/HOR. Although Pt loading on the anode is 4 times less than it is on the cathode,[65] its amount still contributes significantly to the current noncompetitive prices of proton exchange membrane fuel cells. The overpotential requirements for HER and HOR are identical because they involve only one electrochemical step (intermediate), and hence, the potential energy profile is symmetrical. In other words, the same catalyst could, in principle, be used for both reactions. In this last section we will discuss if some of the catalysts reported in this study could be potentially used as viable replacements for platinum for HER/HOR.

A good HER/HOR catalyst should have G(H*) as close as possible to 0 eV. Looking at Table 2, there are quite a few candidates with promising H* binding energies (Rh, Ir, Au, and Co). The Rh-functionalized porphyrin-like graphene appears to be the best candidate with a G(H*) binding of 0.15 eV. It is important to note that since a single metal atom cannot simultaneously bind two hydrogen atoms, the hydrogen evolution reaction would be forced through the Heyrovsky step. The Heyrovsky step has a 2 times higher barrier than the Tafel step, assuming that the same water bilayer structure would form at the graphene/water interface as on metal surfaces.[59] Kinetic limitations might therefore make these catalysts less active than the metals with similar thermodynamic barriers. HER would proceed unhindred at the potentials relevant for CRR as the charge transfer barriers would become smaller.[59] Finally, it is important to stress that Rh, Co, and Ir seem to be the best porphyrin catalysts for a range of electrochemical reactions, not just for the ones investigated in this work, but also, for instance, for the oxygen reduction reaction.[55]

IV. CONCLUSIONS

In summary, we have assessed the catalytic activity of the metal-functionalized porphyrin-like structures toward the electrochemical reduction of CO_2 and CO. This study was prompted by recent findings on Cu(211).[18] The major obstacle preventing efficient CO_2 reduction was hydrogen poisoning of the active site. This turned out to be a general setback regardless of the metal atom in the porphyrin ring. We suggest a way to circumvent this problem, namely, reducing CO rather than CO_2, as CO* competes better than COOH* with H* for the active sites. Moreover, on the basis of the linear relationships among the reaction intermediates, we have constructed volcano plots which helped us identify the best catalyst candidate: Rh-functionalized pophyrin-like graphene featuring an overpotential of 0.22 V for CO reduction to methanol. This is much lower than the overpotential on the extended metal surfaces; however, the potential needs to be cycled so that CO can be adsorbed in one potential range and reduced in another, making sure water does not dissociate when the potential is cycled positively. Finally, we have also

dx.doi.org/10.1021/jp306172k | J. Phys. Chem. C 2013, 117, 9187−9195

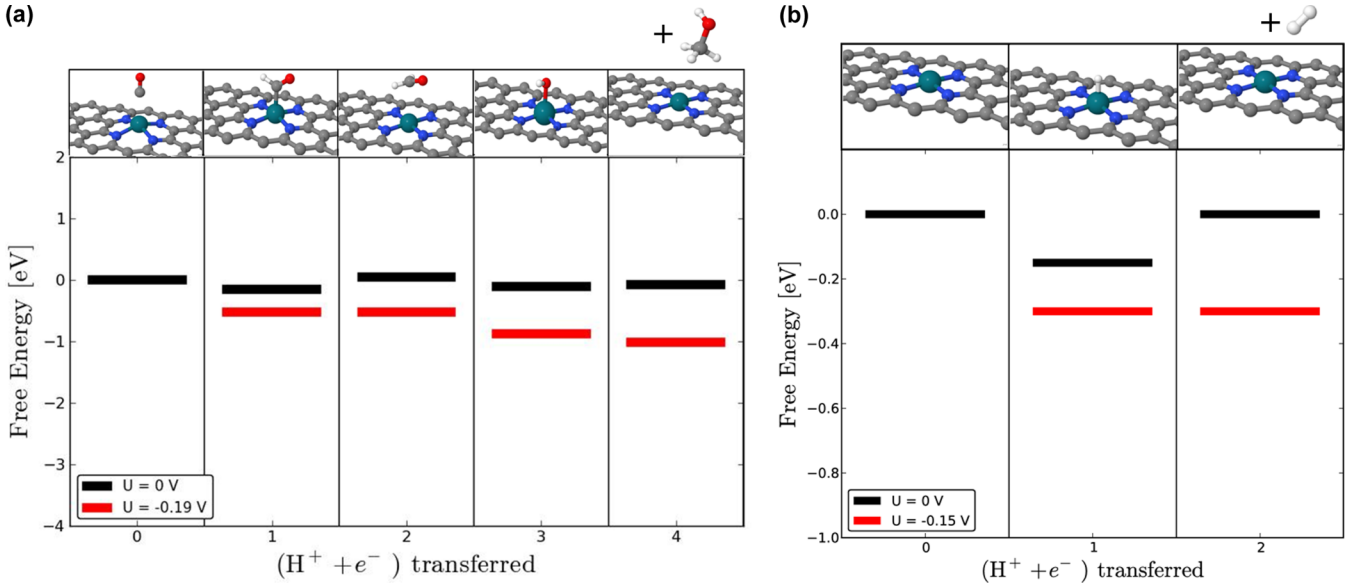

Figure 5. Free energy diagrams for (a) the CO_2 reduction reaction and (b) hydrogen evolution/oxidation reaction on Rh−porphyrin-like functionalized graphene, respectively. The black and red lines denote the free energy levels at 0 V and at the potentials at which all the reaction steps are downhill in free energy.

Table 2. Calculated Overpotentials for the Hydrogen Evolution/Oxidation Reaction

metal	overpotential (V)
Cu	−1.70
Ag	−0.68
Au	−0.23
Ni	−1.67
Pd	−2.05
Pt	−1.77
Co	−0.26
Rh	0.15
Ir	0.28
Fe	−0.45
Ru	0.35
Os	0.57
Mg	−1.35
B	1.60
Al	0.38
Ga	0.77

briefly examined the catalytic activity of the metal−porphyrins for HER/HOR. Even though there are a few candidates with promising overpotentials, it is still unclear whether these systems would, in reality, be that active due to severe kinetic limitations.

■ ASSOCIATED CONTENT

Ⓢ Supporting Information

Sensitivity analysis of CO_2 and CO corrections derived from a set of reactions containing CO and CO_2 molecules. Tables with the most stable spin states and free binding energies for different intermediates. DOS analysis. This material is available free of charge via the Internet at http://pubs.acs.org.

■ AUTHOR INFORMATION

Corresponding Author

*E-mail: jross@fysik.dtu.dk. Phone: (+45) 45-253-166. Fax: (+45) 45-932-399.

Notes

The authors declare no competing financial interest.

■ ACKNOWLEDGMENTS

The Catalysis for Sustainable Energy initiative is funded by the Danish Ministry of Science, Technology and Innovation. Support from the Danish Center for Scientific Computing, the Danish Council for Technology and Innovation's FTP program, and the Strategic Electrochemistry Research Center is gratefully acknowledged. We also acknowledge Juan Maria Garcia Lastra for fruitful discussions.

■ ABBREVIATIONS

DFT, density functional theory; DOS, density of states; CRR, CO_2 reduction reaction; HER, hydrogen evolution reaction; HOR, hydrogen oxidation reaction; PDS, potential determining step

■ REFERENCES

(1) Lewis, N. S.; Nocera, D. G. Powering the Planet: Chemical Challenges in Solar Energy Utilization. *Proc. Natl. Acad. Sci. U. S. A.* **2006**, *103*, 15729−15735.

(2) Gattrel, M.; Gupta, N.; Co, A. A Review of the Aqueous Electrochemical Reduction of CO_2 to Hydrocarbons at Copper. *J. Electroanal. Chem.* **2006**, *594*, 1−19.

(3) Hori, Y.; Kikuchi, K.; Murata, A.; Suzuki, S. Production of Methane and Ethylene in Electrochemical Reduction of Carbon-Dioxide at Copper Electrode in Aqueous Hydrogencarbonate Solution. *Chem. Lett.* **1986**, *15*, 897−898.

(4) Hori, Y.; Murata, A.; Takahashi, R.; Suzuki, S. Electroreduction of CO to CH_4 and C_2H_4 at a Copper Electrode in Aqueous Solutions at Ambient Temperature and Pressure. *J. Am. Chem. Soc.* **1987**, *109*, 5022−5023.

(5) Hori, Y.; Murata, A.; Takahashi, R. Formation of Hydrocarbons in the Electrochemical Reduction of Carbon-Dioxide at a Copper Electrode in Aqueous-Solution. *J. Chem. Soc., Faraday Trans.* **1989**, *85*, 2309−2326.

(6) Hori, Y.; Wakebe, H.; Tsukamoto, T.; Koga, O. Electrocatalytic Process of CO Selectivity in Electrochemical Reduction of CO_2 at

Metal-Electrodes in Aqueous-Media. *Electrochim. Acta* **1994**, *39*, 1833−1839.
(7) Hori, Y.; Takahashi, R.; Yoshinami, Y.; Murata, A. Electrochemical Reduction of CO at a Copper Electrode. *J. Phys. Chem. B* **1997**, *101*, 7075−7081.
(8) Hori, Y. *Modern Aspects of Electrochemistry*; Springer: New York, 2008; Vol. 42, Chapter 3, pp 89−189.
(9) Benson, E. E.; Kubiak, C. P.; Sathrum, A. J.; Smieja, J. M. Electrocatalytic and Homogeneous Approaches to Conversion of CO2 to Liquid Fuels. *Chem. Soc. Rev.* **2009**, *38*, 89−99.
(10) Roy, S. C; Varghese, O. K.; Paulose, M.; Grimes, C. A. Toward Solar Fuels: Photocatalytic Conversion of Carbon Dioxide to Hydrocarbons. *ACS Nano* **2010**, *4*, 1259−1278.
(11) Darensbourg, D. J. Chemistry of Carbon Dioxide Relevant to Its Utilization: A Personal Perspective. *Inorg. Chem.* **2010**, *49*, 10765−10780.
(12) Barton Cole, E.; Lakkaraju, P. S.; Rampulla, D. M.; Morris, A. J.; Abelev, E.; Bocarsly, A. B. Using a One-Electron Shuttle for the Multielectron Reduction of CO_2 to Methanol: Kinetic, Mechanistic, and Structural Insights. *J. Am. Chem. Soc.* **2010**, *132*, 11539−11551.
(13) Le, M.; Ren, M.; Zhang, Z.; Sprunger, P. T.; Kurtz, R. L.; Flake, J. C. Electrochemical Reduction of CO_2 to CH_3OH at Copper Oxide Surfaces. *J. Electrochem. Soc.* **2011**, *158*, E45−E49.
(14) Whipple, D. T.; Kenis, P. J. A. Prospects of CO_2 Utilization via Direct Heterogeneous Electrochemical Reduction. *J. Phys. Chem. Lett.* **2010**, *1*, 3451−3458.
(15) Schouten, K. J. P.; Kwon, Y.; van der Ham, C. J. M.; Qin, Z.; Koper, M. T. M. A New Mechanism for the Selectivity to C-1 and C-2 Species in the Electrochemical Reduction of Carbon Dioxide on Copper Electrodes. *Chem. Sci.* **2011**, *2*, 1902−1909.
(16) Schouten, K. J. P.; Qin, Z.; Gallent, E. P.; Koper, M. T. M. Two Pathways for the Formation of Ethylene in CO Reduction on Single-Crystal Copper Electrodes. *J. Am. Chem. Soc.* **2012**, *134*, 9864−9867.
(17) Chaplin, R. P. S; Wragg, A. A. Effects of Process Conditions and Electrode Material on Reaction Pathways for Carbon Dioxide Electroreduction with Particular Reference to Formate Formation. *J. Appl. Electrochem.* **2003**, *33*, 1107−1123.
(18) Peterson, A. A.; Abild-Pedersen, F.; Studt, F.; Rossmeisl, J.; Nørskov, J. K. How Copper Catalyzes the Electroreduction of Carbon Dioxide into Hydrocarbon Fuels. *Energy Environ. Sci.* **2010**, *3*, 1311−1315.
(19) Peterson, A. A.; Nørskov, J. K. Activity Descriptors for CO_2 Electroreduction to Methane on Transition-Metal Catalysts. *J. Phys. Chem. Lett.* **2012**, *3*, 251−258.
(20) Durand, W. J.; Peterson, A. A.; Studt, F.; Abild-Pedersen, F.; Nørskov, J. K. Structure Effects on the Energetics of the Electrochemical Reduction of CO_2 by Copper Surfaces. *Surf. Sci.* **2011**, *605*, 1354−1359.
(21) Kim, J. J.; Summers, D. P., Jr.; Frese, K. W. Reduction of CO_2 and CO to Methane on Cu Foil Electrodes. *J. Electroanal. Chem.* **1988**, *245*, 223−244.
(22) DeWulf, D. W.; Jin, T.; Baard, A. J. Electrochemical and Surface Studies of Carbon-Dioxide Reduction to Methane and Ethylene at Copper Electrodes in Aqueous-Solutions. *J. Electrochem. Soc.* **1989**, *136*, 1686−1691.
(23) Nørskov, J. K.; Rossmeisl, J.; Logadottir, A.; Lindqvist, L.; Kitchin, J. R.; Bligaard, T.; Jonsson, H. Origin of the Overpotential for Oxygen Reduction at a Fuel-Cell Cathode. *J. Phys. Chem. B* **2004**, *108*, 17886−17892.
(24) Lee, D. H.; Lee, W. J.; Lee, W. J.; Kim, S. O.; Kim, Y.-H. Theory, Synthesis, and Oxygen Reduction Catalysis of Fe-Porphyrin-Like Carbon Nanotube. *Phys. Rev. Lett.* **2011**, *106*, 175502.
(25) Titov, A.; Zapol, P.; Král, P.; Liu, D.-J.; Iddir, H.; Baishya, K.; Curtiss, L. A. Catalytic Fe-xN Sites in Carbon Nanotubes. *J. Phys. Chem. C* **2009**, *113*, 21629−21634.
(26) Kattel, S.; Atanassov, P.; Kiefer, B. Stability, Electronic and Magnetic Properties of In-Plane Defects in Graphene: A First-Principles Study. *J. Phys. Chem. C* **2012**, *116*, 8161−8166.
(27) Kamat, P. V. Graphene-Based Nanoassemblies for Energy Conversion. *J. Phys. Chem. Lett.* **2011**, *2*, 242−251.
(28) Qu, L.; Liu, Y.; Baek, J.-B.; Dai, L. Nitrogen-Doped Graphene as Efficient Metal-Free Electrocatalyst for Oxygen Reduction Reaction. *ACS Nano* **2010**, *4*, 1321−1326.
(29) Kamat, P. V. Graphene-Based Nanoarchitectures. Anchoring Semiconductor and Metal Nanoparticles on a Two-Dimensional Carbon Support. *J. Phys. Chem. Lett.* **2010**, *1*, 520−527.
(30) Feng, H.; Ma, J.; Hu, Z. Nitrogen-Doped Carbon Nanotubes Functionalized by Transition Metal Atoms: A Density Functional Study. *J. Mater. Chem.* **2010**, *20*, 1702−1708.
(31) Ziegelbauer, J. M.; Olson, T. S.; Pylypenko, S.; Alamgir, F.; Jaye, C.; Atanassov, P.; Mukerjee, S. Direct Spectroscopic Observation of the Structural Origin of Peroxide Generation from Co-Based Pyrolyzed Porphyrins for ORR Applications. *J. Phys. Chem. C* **2008**, *112*, 8839−8849.
(32) Olson, T. S.; Pylypenko, S.; Fulghum, J. E.; Atanassov, P. Bifunctional Oxygen Reduction Reaction Mechanism on Non-Platinum Catalysts Derived from Pyrolyzed Porphyrins. *J. Electrochem. Soc.* **2010**, *157*, B54−B63.
(33) Li, Y.; Zhou, W.; Wang, H.; Xie, L.; Liang, Y.; Wei, F.; Idrobo, J.-C.; Pennycook, S. J.; Dai, H. An Oxygen Reduction Electrocatalyst Based on Carbon Nanotube-Graphene Complexes. *Nat. Nanotechnol.* **2012**, *7*, 394−400.
(34) Ramirez, G.; Ferraudi, G.; Chen, Y.-Y.; Trollund, E.; Villagra, D. Enhanced Photoelectrochemical Catalysis of CO(2) Reduction Mediated by a Supramolecular Electrode of Packed Co(II)-(tetrabenzoporphyrin). *Inorg. Chim. Acta* **2009**, *362*, 5−10.
(35) Ogura, K.; Yoshida, I. Electrocatalytic Reduction of CO_2 to Methanol. 9. Mediation with Metal Porphyrins. *J. Mol. Catal.* **1988**, *47*, 51−57.
(36) Bhugun, I.; Lexa, D.; Saveant, J. M. Catalysis of the Electrochemical Reduction of Carbon Dioxide by Iron(0) Porphyrins: Synergystic Effect of Lewis Acid Cations. *J. Phys. Chem.* **1996**, *100*, 19981−19985.
(37) Bhugun, I.; Lexa, D.; Saveant, J. M. Catalysis of the Electrochemical Reduction of Carbon Dioxide by Iron(0) Porphyrins: Synergystic Effect of Weak Bronsted Acids. *J. Am. Chem. Soc.* **1996**, *118*, 1769−1776.
(38) Hammer, B.; Hansen, L. B.; Nørskov, J. K. Improved Adsorption Energetics within Density-Functional Theory Using Revised Perdew-Burke-Ernzerhof Functionals. *Phys. Rev. B* **1999**, *59*, 7413−7421.
(39) Mortensen, J. J.; Hansen, L. B.; Jacobsen, K. W. Real-Space Grid Implementation of the Projector Augmented Wave Method. *Phys. Rev. B* **2005**, *71*, 035109.
(40) Enkovaara, J.; Rostgaard, C.; Mortensen, J. J.; Chen, J.; Dulak, M.; Ferrighi, L.; Gavnholt, J.; Glinsvad, C.; Haikola, V.; Hansen, H. A.; et al. Electronic Structure Calculations with GPAW: A Real-Space Implementation of the Projector Augmented-Wave Method. *J. Phys.: Condens. Matter* **2010**, *22*, 253202.
(41) Atomic Simulation Environment (ASE); Center for Atomic-scale Materials Design (CAMD), Technical University of Denmark, Lyngby. https://wiki.fysik.dtu.dk/ase.
(42) Dhanasekaran, T.; Grodkowski, J.; Neta, P.; Hambright, P.; Fujita, E. *p*-Terphenyl-Sensitized Photoreduction of CO_2 with Cobalt and Iron Porphyrins. Interaction between CO and Reduced Metalloporphyrins. *J. Phys. Chem. A* **1999**, *103*, 7742−7748.
(43) Grodkowski, J.; Dhanasekaran, T.; Neta, P.; Hambright, P.; Brunschwig, B. S.; Shinozaki, K.; Fujita, E. Reduction of Cobalt and Iron Phthalocyanines and the Role of the Reduced Species in Catalyzed Photoreduction of CO_2. *J. Phys. Chem. A* **2000**, *104*, 11332−11339.
(44) Kadish; K. M.; Royal, G.; Van Caemelbecke, E.; Gueletti, L. In *The Porphyrin Handbook*; Kadish, K. M., Smith, K. M., Guilard, R., Eds.; Academic Press: Boston, 2000; Vol. 9, pp 1−219.
(45) Lefévre, M.; Proietti, E.; Jaouen, F.; Dodelet, J.-P. Iron-Based Catalysts with Improved Oxygen Reduction Activity in Polymer Electrolyte Fuel Cells. *Science* **2009**, *324*, 71−74.

(46) Gupta, S.; Tryk, D.; Bae, I.; Aldred, W.; Yeager, E. Heat-Treated Polyacrylonitrile-Based catalysts for Oxygen Reduction Reaction. *J. Appl. Electrochem.* **1989**, *19*, 19−27.
(47) Calle-Vallejo, F.; Martínez, J. I.; García-Lastra, J. M.; Abad, E.; Koper, M. T. M. Oxygen Reduction and Evolution at Single-Metal Active Sites: Comparison between Functionalized Graphitic Materials and Protoporphyrins. *Surf. Sci.* **2013**, *607*, 47−53.
(48) Leung, K.; Rempe, S. B.; Schultz, P. A.; Sproviero, E. M.; Batista, V. S.; Chandross, M. E.; Medforth, C. J. Density Functional Theory and DFT+U study of Transition Metal Porphines Adsorbed on Au(111) Surfaces and Effects of Applied Electric Fields. *J. Am. Chem. Soc.* **2006**, *128*, 3659−3668.
(49) Leung, K. Transition-Metal Ion Impurities in $KTaO_3$. *Phys. Rev. B* **2002**, *65*, 012102.
(50) Reiher, M.; Salomon, O.; Hess, B. A. Dinuclear Diazene Iron and Ruthenium Complexes as Models for Studying Nitrogenase Activity. *Theor. Chem. Acc.* **2001**, *107*, 48.
(51) Reiher, M. Theoretical Study of the $Fe(phen)_2(NCS)_2$ Spin-Crossover Complex with Reparametrized Density Functionals. *Inorg. Chem.* **2002**, *41*, 6928.
(52) Cramer, C. J.; Truhlar, D. G. Density Functional Theory for Transition Metals and Transition Metal Chemistry. *Phys. Chem. Chem. Phys.* **2009**, *11*, 10757−10816.
(53) Nielsen, I. M. B.; Leung, K. Cobalt-Porphyrin Catalyzed Electrochemical Reduction of Carbon Dioxide in Water. 1. A Density Functional Study of Intermediates. *J. Phys. Chem. A* **2010**, *114*, 10166−10173.
(54) Leung, K.; Nielsen, I. M. B.; Sai, N.; Medforth, C.; Shelnutt, J. A. Cobalt-Porphyrin Catalyzed Electrochemical Reduction of Carbon Dioxide in Water. 2. Mechanism from First Principles. *J. Phys. Chem. A* **2010**, *114*, 10174−10184.
(55) Calle-Vallejo, F.; Martínez, J. I.; Rossmeisl, J. Density Functional Studies of Functionalized Graphitic Materials with Late Transition Metals for Oxygen Reduction Reaction. *Phys. Chem. Chem. Phys.* **2011**, *13*, 15639−15643.
(56) Karlberg, G. S.; Rossmeisl, J.; Nørskov, J. K. Estimations of Electric Field Effects on the Oxygen Reduction Reaction based on the Density Functional Theory. *Phys. Chem. Chem. Phys.* **2007**, *9*, 5158−5161.
(57) Karlberg, G. S.; Jaramillo, T. F.; Skúlason, E.; Rossmeisl, J.; Bligaard, T.; Nørskov, J. K. Cyclic Voltammograms for H on Pt(111) and Pt(100) from First Principles. *Phys. Rev. Lett.* **2007**, *99*, 126101.
(58) Tripkovic, V.; Skúlason, E.; Siahrostami, S.; Nørskov, J. K.; Rossmeisl, J. The Oxygen Reduction Reaction Mechanism on Pt(111) from Density Functional Theory Calculations. *Electrochim. Acta* **2010**, *55*, 7975−7981.
(59) Skúlason, E.; Tripkovic, V.; Björketun, M. E.; Gudmundsdóttir, S.; Karlberg, G.; Rossmeisl, J.; Bligaard, T.; Jónsson, H.; Nørskov, J. K. Modeling the Electrochemical Hydrogen Oxidation and Evolution Reactions on the Basis of Density Functional Theory Calculations. *J. Phys. Chem. C* **2010**, *114*, 18182−18197.
(60) Koper, M. T. M. Thermodynamic Theory of Multi-Electron Transfer Reactions: Implications for Electrocatalysis. *J. Electroanal. Chem.* **2011**, *660*, 254−260.
(61) Abild-Pedersen, F.; Greeley, J.; Studt, F.; Rossmeisl, J.; Munter, T. R.; Moses, P. G.; Skúlason, E.; Bligaard, T.; Nørskov, J. K. Scaling Properties of Adsorption Energies for Hydrogen-Containing Molecules on Transition-Metal Surfaces. *Phys. Rev. Lett.* **2007**, *99*, 016105.
(62) Hammer, B.; Nørskov, J. K. Electronic Factors Determining the Reactivity of Metal Surfaces. *Surf. Sci.* **1995**, *343*, 211−220.
(63) Rossmeisl, J.; Qu, Z.-W.; Zhu, H.; Kroes, G.-J.; Nørskov, J. K. Electrolysis of Water on Oxide Surfaces. *J. Electroanal. Chem.* **2007**, *607*, 83−89.
(64) Ferrin, P.; Nilekar, A. U; Greeley, J.; Mavrikakis, M.; Rossmeisl, J. Reactivity Descriptors for Direct Methanol Fuel Cell Anode Catalysts. *Surf. Sci.* **2008**, *602*, 3424−3431.
(65) Gasteiger, H. A.; Kocha, S. S.; Sompalli, B.; Wagner, F. T. Activity Benchmarks and Requirements for Pt, Pt-Alloy, and Non-Pt Oxygen Reduction Reaction Catalysts for PEMFCs. *Appl. Catal., B* **2005**, *56*, 9−35.